ELSEVIER

A new approach to flow-field measurement—A view of Doppler global velocimetry techniques

R. W. Ainsworth, S. J. Thorpe, and R. J. Manners
Department of Engineering Sciences, Oxford University, Oxford, UK

Nonintrusive techniques for determining velocities in fluid flowfields, based on the use of laser technology, have been the subject of much research over the last three decades. Many of these techniques, such as laser-Doppler-anemometry (LDA) and laser-two-focus-anemometry (L2F), have been based on point-wise measurements until the advent, in the last decade, of particle image velocimetry (PIV). There is much interest in pursuing the goal of nonintrusive, whole-field velocity measurements, although such techniques are still some way from maturity. A new technique has recently emerged to challenge the position of PIV: the technique of Doppler global velocimetry (DGV). This paper outlines the origins of the technique, the physical principles involved, and the potential advantages of DGV over PIV. A review is made of the technology used by the small number of groups researching this new method, drawing comparisons between the major aspects of their differing techniques. Finally, examples are given of "test case" measurements of two well-established velocity fields: those of a rotating disc, and those in a subsonic open jet.

Keywords: Doppler global velocimetry; flow-field measurement

Introduction

The last two decades have seen an upsurge in the number of techniques being developed in experimental fluid mechanics to allow determination of whole fields of scalar and vector quantities such as density and velocity, aimed at replacing more traditional point-wise techniques. The impetus for this has perhaps been provided by the siren-like qualities of images emanating from computational fluid dynamical (CFD) analysis, where there is a desire to verify the performance of codes in modelling the detailed fluid mechanics of complex flows. Such experimental techniques for vector fields have included nuclear-magnetic-resonance imaging (Lee et al. 1987), laser-induced fluorescence, molecular-tracking (Miles et al. 1989), laser-speckle velocimetry, and particle image velocimetry (PIV) (Adrian 1991).

Of these techniques, it is PIV that has commanded the most attention, particularly for internal transonic flows such as those encountered in gas turbines. Particle image velocimetry uses a double-pulse laser to illuminate a measurement plane within the flow, and scattered light from seeding particles present is imaged onto a photographic emulsion. The double exposures recorded by the emulsion are subsequently analysed to determine the distance travelled by a particular particle between pulses.

Whilst the PIV technique undoubtedly offers a major advance for the experimenter, it is not without its disadvantages. Firstly, it is necessary to produce optics that will enable individual seeding particles to be imaged. In transonic flows, these may be of order 0.5-μm diameter. Additionally, the same particles must be imaged twice. Secondly, considerable off-line processing is required to deconvolve the double image into a velocity field. Thirdly, three-dimensional (3-D) velocity information is difficult to retrieve. Nevertheless, much effort continues to be made to enhance existing techniques—PIV will continue to be an important technique for many years to come.

The main purpose of this paper is, however, to review the new technique of Doppler global velocimetery (DGV), which appears to offer much promise for one-shot, 3-D, whole-field velocity determination. Doppler global velocimetry is a whole-field technique, which measures the change in frequency of laser light reflected from seeding particles embedded in a flow field with respect to the incident frequency. This change in frequency (shift) is caused by the Doppler effect, Komine and Brosnan (1991) being the first to realise it could be determined by using a frequency-to-intensity converting optical filter, in the form of an iodine vapour cell. Iodine vapour acts as a radiation-absorbing medium, with an absorption coefficient strongly dependent on frequency. As is demonstrated later in greater detail, on the scale of the bandwidth of an iodine absorption feature, the incident laser light may be considered to be monochromatic. By imaging the whole field through the iodine cell with a camera, an image would be obtained whose intensity corresponds to the frequency shift, which, when used with a (frequency-to-velocity) calibration of the iodine cell, would yield a whole-field velocity map. Using laser light sheet illumination and imaging optics, DGV measures the global velocity within a two-dimensional (2-D) "slice" of the seeded flow—but, although the "slice" is 2-D, 3-D velocities can

Address reprint requests to Dr. R. W. Ainsworth, Department of Engineering Science, Oxford University, Parks Road, OX1 3PJ, Oxford, UK.

Received 10 March 1966; accepted 15 October 1996

Int. J. Heat and Fluid Flow 18: 116–130, 1997

655 Avenue of the Americas, New York, NY 10010

0142-727X/97/$17.00
PII S0142-727X(96)00147-X

be obtained within it. In addition, it is unnecessary to image every seeding particle in the flow. If, for example, a CCD camera is used to record the images, the reflected light from a number of particles would fall on one pixel of the camera array, the number depending on seeding density and image scaling. Thus, distinct advantages over PIV seem possible: only one shot of the flow field is required; 3-D information is readily available; data processing is easier; and the requirements for the imaging optics are much less stringent.

Whilst the principle of DGV seems simple and elegant, in practice, complex arrangements are necessary if accurate measurements (absolute velocities) are to be obtained. In the following section, details of the current practice at Oxford and elsewhere are discussed.

Doppler global velocimetry technique

Yeh and Cummins (1964) were the first to exploit the shift in optical frequency of scattered light from objects passing through a laser beam. They used it, in a point measurement-based system, to develop the reference beam laser Doppler velocimeter. The fundamental Doppler shift equation they used is also the cornerstone of the DGV technique. The shift in frequency seen in the light scattered from an object moving with velocity $\mathbf{V}$ depends on both the incident radiation direction and the observation direction (Figure 1) as follows:

$$\Delta f = \frac{(\hat{\mathbf{o}} - \hat{\mathbf{i}}) \cdot \mathbf{V}}{\lambda_o} \tag{1}$$

where λ_o is the incident light wavelength, and Δf the Doppler shift.

This vector equation demonstrates that the Doppler shift is sensitive to one particular component of velocity; namely, in the direction of $\hat{\mathbf{o}} - \hat{\mathbf{i}}$. This relation implies that the magnitude of the Doppler shift is a function of this direction, and consequently, three components of velocity can be derived on this basis, either by altering the observation direction or the illumination direction. The maximum shift is of order 2 MHz per ms^{-1}.

Komine et al. (1991) demonstrated the use of an iodine vapour cell as a device for measuring Doppler-shift frequencies over an extended 2-D area and introduced the acronym of DGV. Iodine, like other halogens, has many absorption lines throughout the visible spectrum, typically a few GHz in width at room temperature. Some of these lines coincide with the frequency of emission of common lasers, such as the 514.5-nm emission of the argon ion laser and the 532-nm emission of the frequency doubled neodymium YAG (Nd:YAG) laser. The laser light source for DGV measurements needs to have a narrow line width in comparison with the width of the iodine absorption feature. This is achieved in argon ion lasers by use of an intracavity etalon and in Nd:YAG pulse lasers by use of injection seeding. Typical bandwidth for such an argon ion laser is of order 2–3 MHz. By tuning the laser emission to the absorption wing, changes in light frequency caused by moving objects can be converted into changes in light intensity by viewing the scattered light through an iodine vapour cell. The transmission of an idealised iodine cell is shown in Figure 2 (a comparison of measured transmission characteristics is given later). In the DGV method, an argon ion laser operating at 514.5 nm is tuned to typically (but not necessarily) 50% transmission through the cell. If that light is incident upon a moving object, the scattered light is frequency shifted according to Equation 1 and will, therefore, have a different level of transmission through the cell, either greater or less than 50%, depending on the direction of object movement. These changes in frequency are also shown in Figure 2. Measurement of that change allows comparison with the known absorption curve to deduce the Doppler shift and, hence, the velocity of the object. To measure velocity over an extended area, beam-expanding optics are employed, and an imaging system is used to capture the scattered light. The method outlined thus far applies to any moving body that scatters light. To measure fluid velocities, it is necessary to seed the flow with scattering sites in much the same way as that used in PIV, LDA, and L2F. The laser beam is expanded using combinations of cylindrical lenses to provide a light sheet that illuminates a single plane of the flow—velocity measurements are obtained within this sheet.

To measure velocity, it is necessary to obtain two images of the same flow region, one viewed through the iodine cell (the signal image), and one viewed directly (the reference image), so that intensity variations across the imaged area can be normalised. Division of these two images on a pixel-by-pixel basis produces a 2-D map of iodine cell transmission over the viewed area—information that is related to the local Doppler shift via the cell calibration. All the work in the United States, emanating from the original research at Northrop (Komine et al. 1991) and through subsequent developments at NASA (Meyers et al. 1991; Meyers 1992, 1994, 1995), have reported the use of two separate CCD cameras for the "reference" and "signal" images. These workers have emphasized obtaining and displaying real-time velocity images in continuously running wind tunnels. The emphasis at Oxford (Ainsworth and Thorpe 1994; Thorpe et al 1995, 1996; Manners et al. 1996), with the transonic turbine flow field

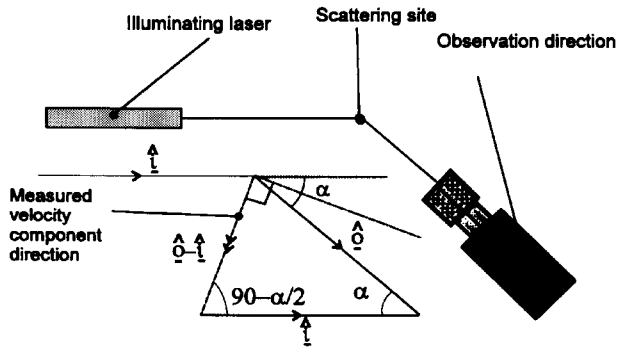

Figure 1 The measured velocity component relative to the laser and observation direction for DGV

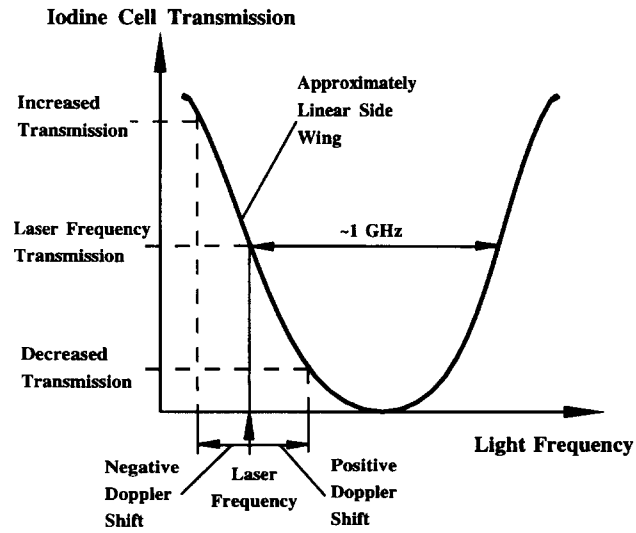

Figure 2 Frequency-to-intensity conversion using molecular absorption

in mind, has, however, been different—absolute velocities are a fundamental requirement, and real-time processing is not a necessity.

Particular features of the Oxford method, which are expounded below, include the use of a single CCD camera to record both signal and reference images, resulting in a greatly simplified system, and the use of an "on-line" method for recording the laser operating frequency at the instant the images are recorded. A second iodine cell was used for this purpose, and data obtained in this way were first published in 1994 (Ainsworth and Thorpe). The approach of others in this respect, again, where absolute results have been called for rather than qualitative flow fields, has been to seek to control actively the emission frequency of the laser (Roehl and Schodl 1994; Ford and Tatam 1994). As discussed above, the signal and reference images must be divided on a pixel-by-pixel basis, and for the real-time system, this must be done by physically adjusting the two image beams so that they are coincident (Komine et al. 1994). With the single-camera system, this, of course, cannot be done, and the images are aligned using image-processing techniques post-test. Manners et al. (1996) emphasize the need for great care in image alignment, demonstrating an accuracy requirement of 0.05 pixels, which can be achieved by image processing, but must be difficult to reach in real-time systems.

The literature contains several applications of DGV to seeded flow fields. Komine and Brosnan (1991) carried out jet flow measurements, whilst Meyers and Komine (1991) and Usry et al. (1992) looked at the vortices above a delta wing at an angle of incidence to the free-stream flow. The use of an argon ion laser for time-averaged results (averaged during the frame integration period of the CCD camera) and Nd:YAG pulse lasers for instantaneous measurements (10 ns flow illumination time) are reported. An iodine cell was employed as the frequency-to-intensity converting filter in all these cases. The use of three separate imaging systems, which allows the determination of three velocity components, has also been established (Komine et al. 1991). Signal-processing schemes for the video data are treated by Meyers et al. (1991).

Detailed system requirements for Doppler global velocimetry measurements

Optical system

As outlined above, two fully synchronised images are required for each DGV measurement. Other workers (Komine et al. 1991; Meyers and Komine 1991) have reported the use of two separate CCD cameras and electronics to obtain simultaneous frame integration between the two (Figure 3). This technique has enabled the capture and display of velocity fields in real time, although the hardware requirements to ensure simultaneous capture have been arduous. Difficulties have been experienced with video-interlacing in establishing which lines of a particular image have been acquired at a certain time. A bore-sight optical configuration was used (Komine et al. 1994) (Figure 4), where the two cameras were aligned so that they were both directed down a common axis. The adjustments required to produce pixel overlap within the accuracy achievable using a hardware-based system included: (1) tilt adjustments of the beamsplitter and steering mirrors; (2) axial translation of one camera to match path lengths from camera to beamsplitter (thus matching magnification); and (3) rotation of one camera about its axis to counteract tilt adjustments (with a 0.5 mrad angular tolerance). The 10-nm passband 532-nm filter was used to reduce the effect of ambient light and was placed in front of the beamsplitter. Cohu Model 4810 8-bit video camera with a CCD array comprising 754×488 pixel elements were used.

The Oxford DGV technique, with its use of a single CCD camera and controlling electronics to capture both reference and signal images, with the field illuminated by a source whose frequency is recorded rather than controlled, enabled the use of developments in imaging technology in the field of astrophysics. Here, the use of ultralow-noise CCD arrays (using Peltier and liquid nitrogen cooling) is increasingly commonplace to record low-intensity images to high fidelity, but not at video-framing rates. A schematic diagram of the resulting DGV optical configuration is shown in Figure 5, with the system in use to measure the velocity of a spinning disc in Figure 6 (both from Ainsworth and Thorpe 1994). The decrease in electrical complexity compared to previously published methods and the assurance of simultaneous image capture are at the expense of halving the potential spatial resolution of the measurement. This may be tolerable, because DGV will yield approximately 80,000 pixels of data over this region (400×200).

The primary lens (50-mm focal length) shown in Figure 5 is used to capture and focus the scattered light into the back focal plane of a second lens (100-mm focal length). The latter is referred to as the transfer lens (Komine et al. 1991), and its function is to produce collimated light. This collimated beam is subsequently incident upon a nonpolarising beam splitter that separates the light between the reference and iodine cell paths. Mirrors guide the light toward a second beam splitter that acts to

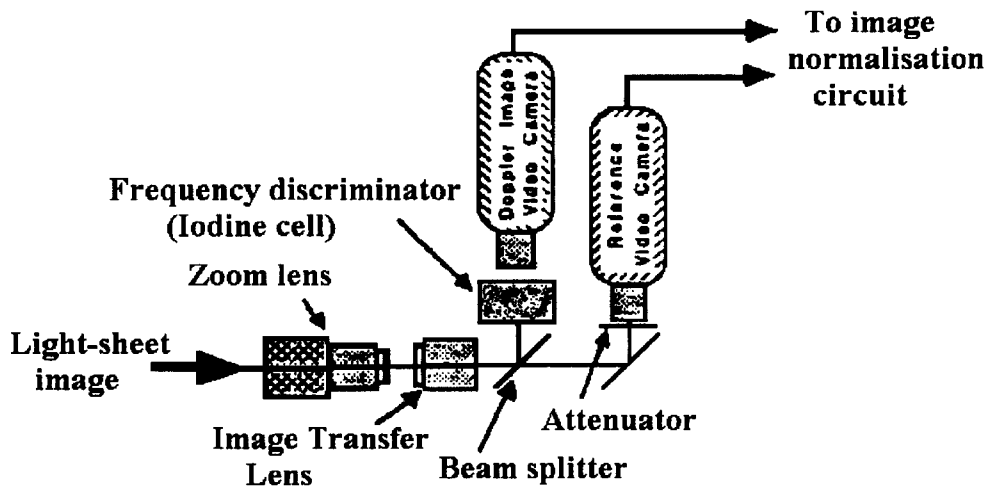

Figure 3 The two-path system (for reference and signal images) of Komine et al. (1991)

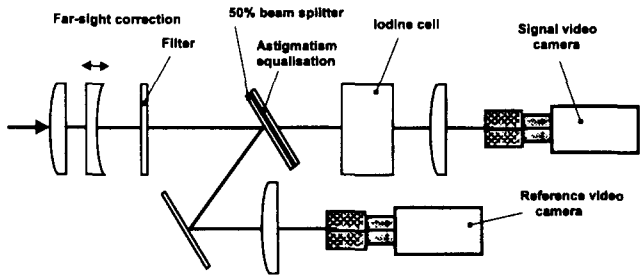

Figure 4 Bore-sight optical system, with separate optical paths for signal and reference images (Komine et al. 1994)

merge the two images into the CCD camera lens, where focus is easily set to infinity. The camera employed uses a Peltier-effect, cooled CCD array with variable integration period, and with a 15-bit A/D converter card interfaced to a PC. After image acquisition on the PC, data are transferred to a workstation for analysis.

In terms of comparing the bore-sight configuration of Komine et al. (1995b) with the Oxford optical system, the Oxford system has the disadvantage in terms of increased transmission losses caused by a greater number of lens components. However, producing identical focusing of both reference and signal images would seem to be much more difficult in the Komine system, where matching of two camera optical systems would be required, compared with setting the single camera lens system to infinity.

Ford and Tatam (1994) have also published whole-field measurements with DGV using a dual camera approach with short-term laser frequency control to 3 MHz, although with temperature changes, movements could be larger (50 MHz per °C. Chan et al. (1995) used a single-camera technique, coupled with a spectrum analyzer capable of resolving laser mode hops (115 MHz). Roehle and Schodl (1994) investigated the DGV technique, but not in the whole-field configuration.

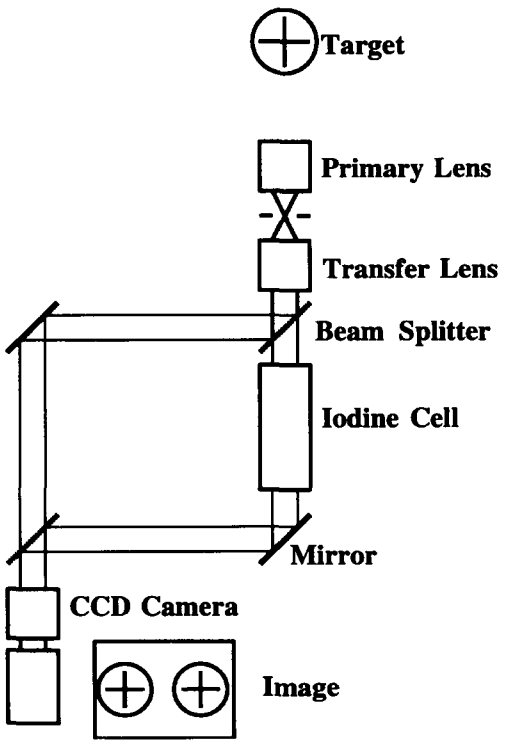

Figure 5 Oxford DGV optical system, using only one camera + recording laser frequency (Ainsworth and Thorpe 1994)

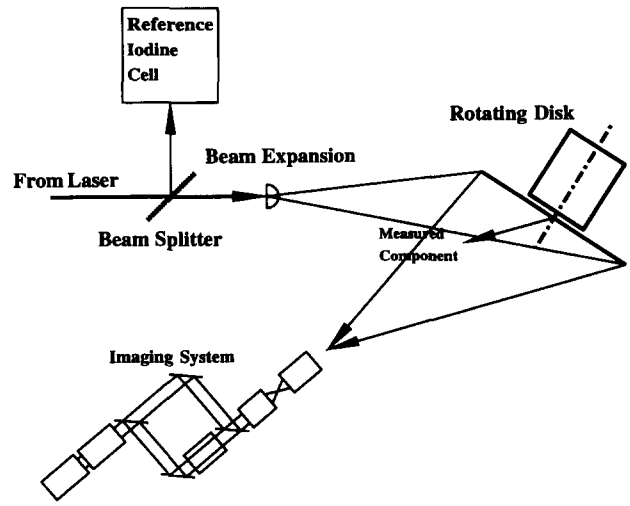

Figure 6 Oxford DGV system used to image the velocity field of a rotating disc (Ainsworth and Thorpe 1994)

Iodine cells

Quantitative DGV measurements rely on accurate knowledge of the iodine cell absorption profile as a function of light frequency in the region of the laser emission (see Figure 2). Examples of iodine cell calibrations are given by a number of workers concerned with DGV measurements, and these are shown below. Komine et al. (1994) show and example of a spectrographic scan of an iodine absorption line in the injection-tuning range of their Nd:YAG laser, at a range of cell temperatures (Figure 7). It can be seen that at the two higher temperatures, the cell has saturated, and complete extinction has been obtained.

When used with an argon ion laser, the spectroscopic area of interest lies around the P13/R15 absorption line system—lines that have significant absorption qualities. The centre frequency of this system is 2-GHz above the centre frequency of the argon 514-nm line. The width of this absorption feature is given as 1.5 GHz by Roehle and Schodl (1994) (defined in terms of full width, half magnitude), the width being mainly due to collisional, Doppler, and hyperfine broadenings. The collision broadening is a function of the iodine vapour pressure (Chan et al. 1995a), whilst the Doppler broadening is a function of temperature. The remaining broadening is contributed by the hyperfine components observed for the P13/T15 lines. Roehle and Schodl make use of this structure, detected using the "so-called 3f-technique of the sub-Doppler spectroscopy," Gill (1979) (the frequency spacing of these hyperfine signals being well known), both in the calibration of their iodine cell by spectroscopic means and in the stabilisation of the frequency of their laser light source. Their resulting calibration is shown in Figure 8, although because most of the hyperfine structure is at a higher frequency than the area of greatest interest (maximum rate of intensity change), some extrapolation presumably is necessary.

Chan et al. (1995a) also show measured iodine vapour transmission at three temperatures, Figure 9, again at argon ion frequency, where movement of the wings of the curve with temperature is evident, at odds with data from the present investigations, Figures 10 and 11, which show collapse with both temperature and cell length. For completeness, comparable data from Ford and Tatum (1994) and Meyers (1995) are given in Figures 12 and 13. Ford comments that the "two discontinuities are due to resets of the laser stabilisation system and occur only

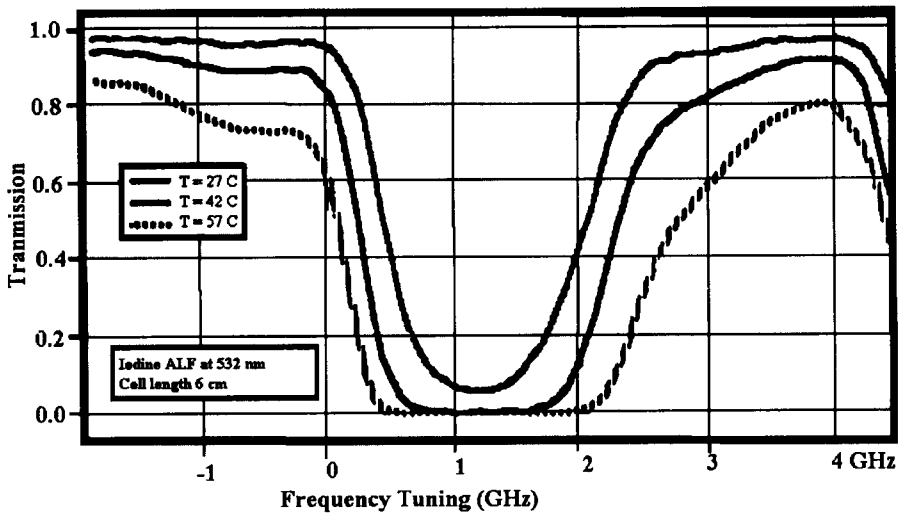

Figure 7 Measured iodine cell transmission profile at three temperatures (Komine et al. 1994)

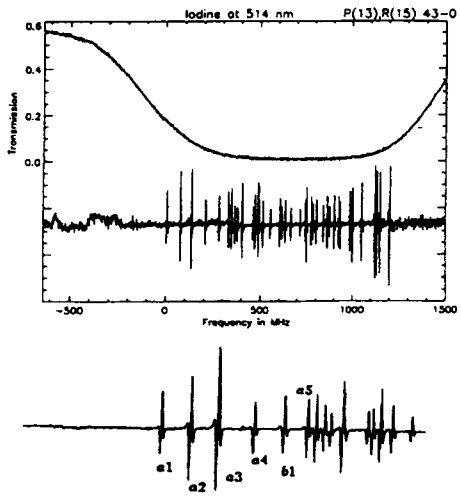

Figure 8 Iodine cell calibration data of Roehle and Schodl (1994), showing position of hyperfine structure

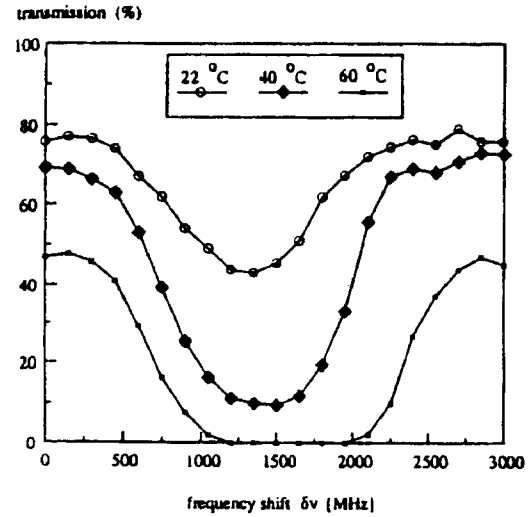

Figure 9 Effect of temperature on iodine cell calibration determined by Chan et al. (1995a)

during scanning over a large frequency range." The Oxford view would certainly be that, in nondimensional terms, the shape of the iodine absorption profile is invariant over a modest temperature range.

It will be seen that the absorption profiles are approximately Gaussian in shape and become progressively deeper as the temperature of the cell is increased. This increase in absorption can be predicted from the known vapour pressure curve of iodine, being directly related to the number density of gas-phase iodine molecules. The width of the absorption feature is approximately 2 GHz and does not appreciably change over the range of temperatures considered. The linear portion of the wings show a sensitivity of around 10 MHz per percentage change in absorption.

In all cases, the cell calibration data must be incorporated into the postprocessing algorithms that determine velocity from the acquired DGV images. In the Oxford system, the philosophy adopted has been to produce a DGV system which has an absolute calibration based on the measured properties of the laser and absorption cell. Others (Meyers and Komine 1991) have described the use of a rotating disc to calibrate the system, but this is not considered by the present authors to be a practical

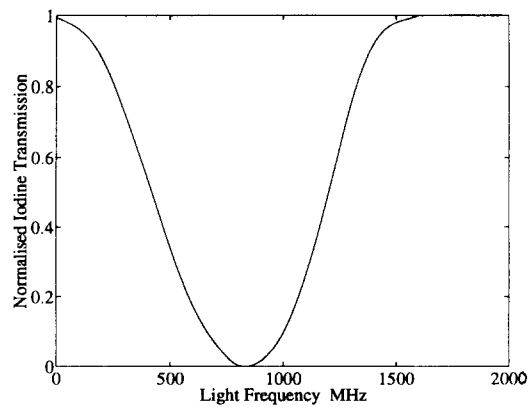

Figure 10 Iodine cell calibration data of the present investigators

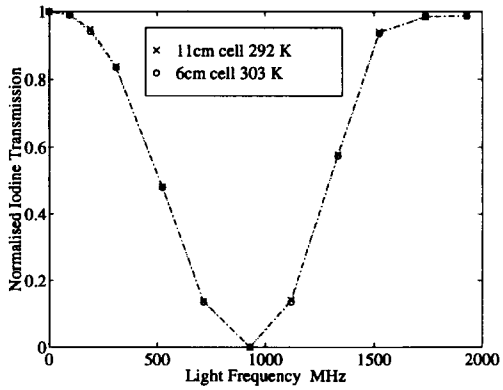

Figure 11 Iodine cell calibration, showing collapse with cell length, and temperature, present investigators

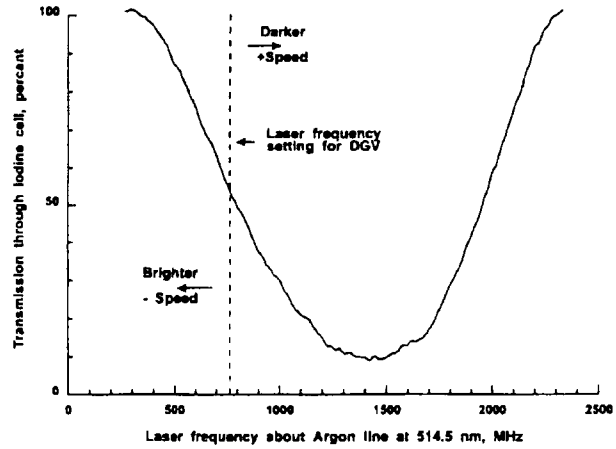

Figure 13 Cell calibration data of Meyers (1995)

proposition once an elaborate application has been constructed. A stable, temperature-controlled reference iodine cell has been developed which is used as a frequency standard to monitor the laser emission continuously. The transmission through the imaging system iodine cell, typically at a different temperature to the reference cell, can then be found from the experimentally determined transmission map.

Properties of the Doppler global velocimetry laser

As has already been explained, the laser source needs to be of narrow linewidth and tunable across an absorption feature of iodine. Also important is the stability of the laser output and, in particular, the ability to determine the laser frequency relative to the absorption feature during acquisition of the DGV images—Doppler shifts will be measured relative to the source frequency. The stability of the argon ion laser employed by Ainsworth and Thorpe (1994) was characterised by two types of frequency fluctuation. The first was due to thermal effects causing the expansion and contraction of the resonator and consequently cavity mirror separation; the second by vibrations which caused a more rapid oscillation in cavity mirror separation. Water-cooling flows were the main cause of the latter phenomena.

The first type of frequency modulation manifested itself as a slow drift of the output frequency between longitudinal resonant modes (separation of 140 MHz) and then a rapid "mode hop" back to the original frequency. This type of feature was particularly pronounced during warm-up, when the resonator was undergoing a temperature rise. After one hour of operation, the period of these mode hops was found to be several minutes, although still a strong function of ambient temperature variations. A Fabry-Perot spectrometer can be used to monitor these modes graphically on an oscilloscope.

This second type of frequency modulation was considered to be an "ac" component superimposed on the first type. Investigation of this phenomena is more important, because it occured on a time-scale comparable to the CCD camera frame integration period. Whereas the investigation of long-time scale fluctuations used a scanning FP, higher-frequency components have been quantified using a different technique. This latter method employed an iodine cell to act as a spectrum analyser. Consider again the shape of the iodine absorption feature shown in Figure 2. The side wings have a region which is linear over a region of approximately 600 MHz. By tuning the output into this region, say 50% transmission, high-frequency modulation of the laser output frequency can be converted into a corresponding change in transmission through the cell. This transmission was monitored using photodiodes, as is done during the iodine cell calibration, and high-speed A/D converters which simultaneously captured the reference and iodine cell intensities. From the iodine cell calibration, these data were used to deduce the level of frequency fluctuation in the laser output. The laser frequency fluctuations over short time-scales found by this technique are shown in Figure 14. Results indicated a 200-Hz oscillation in the output frequency with an amplitude of 10 MHz. In theory, such variations are damaging to the accuracy of the DGV measure-

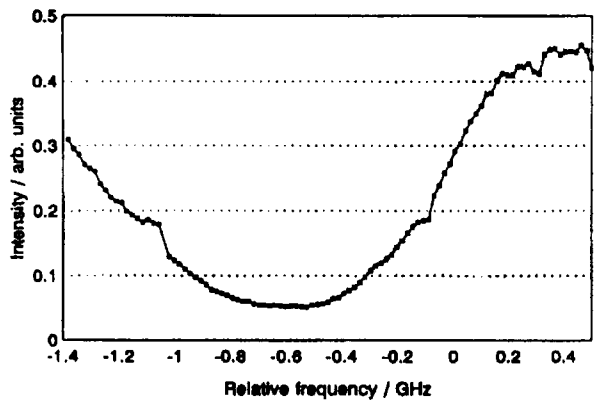

Figure 12 Cell calibration of Ford and Tatam (1994)

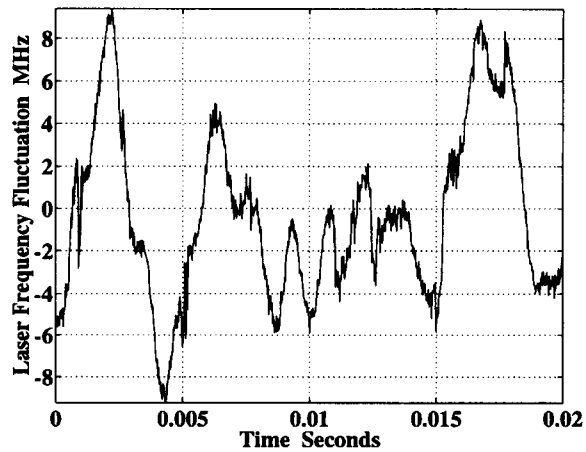

Figure 14 Short-term argon ion laser frequency instability (Ainsworth and Thorpe 1994)

ment, because the variation in laser frequency may represent an error of up to ± 5 ms^{-1} in velocity. However, by monitoring the laser frequency during the integration period of the camera, the effect of the changes can be accounted for when calculating the velocity.

The use of a Nd:YAG pulse laser for instantaneous measurements follows lines similar to those outlined for the argon ion laser used in the Oxford system. The pulse laser is fitted with an injection seeding system that controls the frequency output of the Q-switched resonator. The injection seeder is a narrow linewidth solid-state laser, which is directed into the main cavity and causes the Nd:YAG pulse to build up at that frequency rather than from spontaneous noise. The overall linewidth is Fourier limited to approximately 90 MHz, which is significantly broader than the single-mode argon ion laser already discussed. The effect of this can be calibrated out of the system by monitoring the effective laser emission frequency with a reference iodine cell.

Roehle and Schodl (1994) follow a different and, the present authors believe, possibly unnecessarily complex approach. Rather than measuring the laser emission frequency at any instant, as advocated above, they attempt to keep the laser frequency stable to a high degree during the measurement procedure. Their frequency control system is shown in Figure 15. Here, the rear laser mirror is mounted on a piezo-translator, permitting frequency tuning by traversing the mirror. An optical spectrum analyser is used to measure this frequency, generating an error signal for the (short-term) Proportional Integral controller. Short-term frequency fluctuations are limited to ± 250 kHz. Because the spectrum analyser also has frequency drift, long-term control is provided by detection of the hyperfine structure referred to above.

Sources of error in Doppler global velocimetry systems

Thorpe et al. (1995) outlined the five major sources of error in their DGV measurement. These are explained and quantified in subsequent sections. Quantification was given in terms of apparent Doppler shift because this is the primary measurement. To give an idea of how this would translate into velocity measurement error, for a typical viewing direction, error in frequency would translate into error in velocity at the rate of 2 MHz per ms^{-1}. As far as the planar data are concerned, variations in viewing optical angles subtended at the imaging plane are usually negligible in this context.

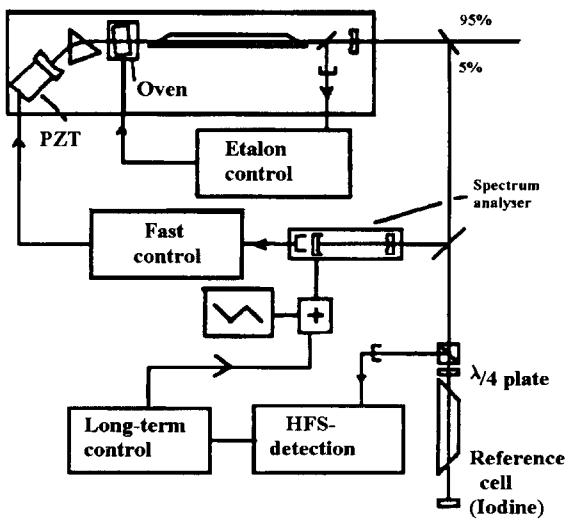

Figure 15 Active laser frequency control system of Roehle and Schodl (1994)

Error of laser frequency determination

Doppler shifts are measured relative to the laser output light frequency during the integration period of the CCD camera. Any error in the measurement of this light frequency relative to the fixed iodine absorption profile will appear as a Doppler-shift frequency offset at every measurement location (pixel), regardless of the actual velocity there. This error is estimated to be ± 3 MHz.

Error in frequency calibration

During calibration of the iodine cell, the variation in laser frequency is estimated to be ± 3 MHz.

Error induced by iodine cell instability

The stability of the iodine cell is critical to successful measurements. In particular, the number density of gaseous phase iodine molecules controls the absorption properties, implying the necessity of accurate temperature control. This is achieved to within ± 0.1 K. Ainsworth and Thorpe (1994) indicated that this typically produces an apparent Doppler shift of ± 2 MHz.

Error introduced by recording system

The recording system, composed of CCD camera together with an A/D convertor, contributes three primary sources of noise. Thermal noise, often called dark current, is a leakage of electrons into the potential wells that form the pixels, but it can be reduced to negligible levels by cooling the CCD chip. A second source is read-out noise and is the error associated with digitisation. This can be reduced by slowing the read-out rate of the camera. The third source is shot noise, an inherent statistical noise. It is well known that shot noise is given as $\sqrt{N}$, where N is the number of electrons in the pixel. For the Peltier-cooled, slow-scan camera use by Thorpe et al. (1995), only shot noise is considered to be a significant term; whereas, the same is not true for a camera operating at video-framing rates. McKenzie (1996), in considering velocimetry uncertainties, also emphasises the role for cooled CCD systems, in terms of noise reduction.

Error due to misalignment of discriminated and reference images

Any error in aligning the two images will lead to an error in the ratio calculated, and this is a particularly strong effect in regions of high-intensity gradient. A method of assessing the error associated with this phenomenon has been constructed and is explained in detail in Thorpe et al. 1995. In the Oxford, work great importance is attached to the quantification and reduction of misalignment errors, which are seen as a major challenge for the DGV technique.

Signal processing

As noted by others (Meyers and Komine 1991; Komine et al. (1991), the two images must be exactly aligned spatially, so that there is an exact correspondence between pixels in the reference image and signal image. Meyers (1995) discusses difficulties experienced at NASA-Langley in large-scale aerodynamic studies using DGV, where at the edges of the seeding smoke plume, large-velocity gradients were observed. He ascribed these to misalignment error, causing problems where intensity gradients were large, and attempted to correct the misalignment by cross-

correlating signal and reference images. This technique may be problematic where differences in intensity profiles (both in the shifted and unshifted images) are to be expected, for obvious reasons. Thorpe et al. (1995) emphasized the need for extreme care regarding alignment, recommending better than a 0.05 pixel error for reducing misalignment error to reasonable proportions. The techniques to achieve this employed by Manners et al. (1996) are briefly given below.

For the single-camera technique, the reference image must be manipulated into the right-hand portion of the CCD frame, while the discriminated image is directed to the left portion. These two images must be transformed to the same coordinate space, so that one may be divided by the other in order to yield a representation of the flow velocity. In this way, corresponding pixels view exactly the same point in the object plane, allowing division of the images on a pixel-by-pixel basis for comparison with the iodine absorption curve. The transformation is arranged so that both images are warped to a regular rectangular grid, allowing the system to be extended to two- and three-component measurements. After the optical system or the light sheet is repositioned, alignment must be undertaken prior to DGV data acquisition. Alignment is performed by the acquisition of three images: an image of a calibration card consisting of a regular array of dots, an image of a plain white card, and an image of a black card. These images are referred to, respectively, as the calibration, normalisation, and black level images. Once processing to ensure image alignment has been achieved, flow measurements can be acquired. Again, three images are required: a data image, together with new normalisation, and black level images.

The alignment process is shown in Figure 16. Firstly, the black level image is subtracted from the calibration image and the normalisation image, in order to remove any spurious black level effects on centroiding accuracy. The calibration image is then divided by the normalisation image, to remove the effects of vignetting in the optics of variation in pixel sensitivity and of nonuniform illumination. The dots are now highlighted by the use of amplitude threshold segmentation, the edges of the image, outside the calibration region, having been masked off.

The segmented image is subjected to a novel algorithm which attempts to reject any lines in the horizontal and vertical directions and to remove high-frequency noise, whilst maintaining the dots themselves. Vertical and horizontal dividing lines are then superimposed on the image, through the spaces in the rectangular array of features, to isolate each dot in a bounding box. The centroid of each of these bounding boxes may then be computed in order to find the coordinates of the centre of the feature thus contained. The advantage of this technique is that centroid detection of the array of dots can be performed entirely automatically, without user intervention. Use of the normalisation image and the black level image ensures that the regions surrounding the dots themselves have a pixel value of zero, and, hence, these regions do not distort the positions of the detected centroids.

Having found the centroids of the dots in the calibration image, the correspondence between the centroids in the discriminated and nondiscriminated parts must be established. The image-processing software has been designed to solve the correspondence problem for the two sets of centroids without user intervention. This can be achieved by the use of a limited cross-correlation to determine the rough offset between the two sets, followed by an iterative matching process. Division of the centroids into bounding boxes also facilitates assignment of the detected centroids to a regular grid. The regular grid of points will form the "target" of the warping transformation, with the actual locations representing the "source." Once correspondence has been established, the warp coefficients may then be computed. Three mathematical algorithms for warping are considered in Manners et al. (1996).

Having performed alignment, the data images must be processed, as shown in Figure 17. The black image is subtracted from both the data image and normalisation images to remove any black offset which may distort the results. The data image is then divided by the normalisation image. Warping is performed, using the coefficients determined as outlined above. The role of

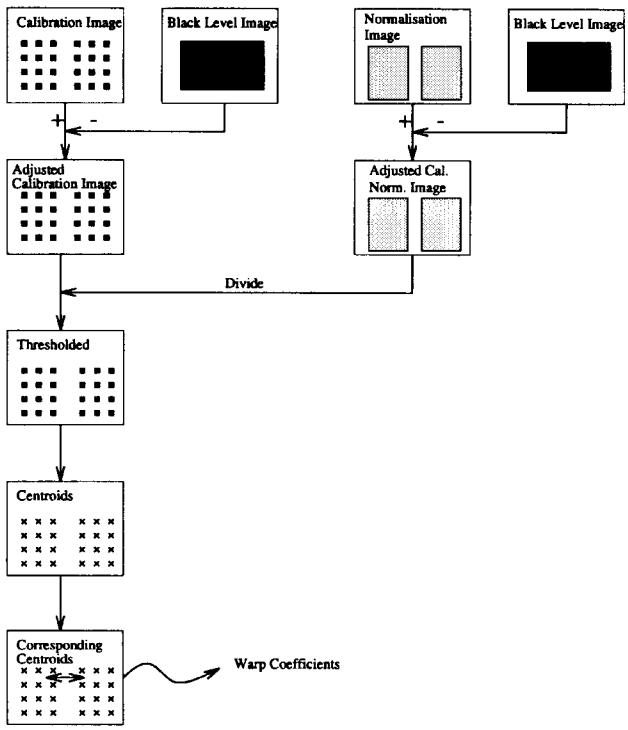

Figure 16 Image acquisition procedures used by Manners et al. (1996)

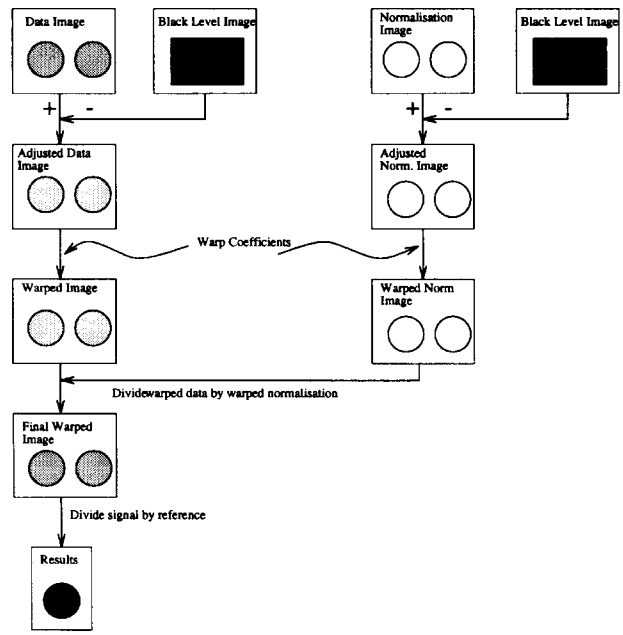

Figure 17 Image-processing procedures to produce measured flow field from the acquired data, used by Manners et al. (1996)

the normalisation image is to account for variations in pixel sensitivity and vignetting in the optical chain. The nondiscriminated and discriminated parts of the image are warped to a regular coordinate system. The warp produces a mapping of the integer coordinates of the pixels, in the warped discriminated part of the image, to noninteger coordinate values, in the original nonwarped discriminated part. Clearly, an interpolation scheme is necessary in order to determine pixel values at each point in the image. Four such schemes are considered by Manners et al. (1996). The effect of the choice of warping technique and interpolation method has been found to be highly significant in terms of the accuracy of DGV measurements attained.

Finally, the discriminated part of the image may be divided by the nondiscriminated part. The iodine cell absorption profile must then be taken into account in order to yield a true velocity measurement.

Particle seeding of flow fields

As far as measurements using the DGV technique are concerned, it is fortunate that there has been a wealth of information emanating from PIV research and, indeed, from the earlier point-wise laser techniques. For transonic and supersonic flows, it may be assumed that the particle dynamic properties must be the same for all techniques.

The response of particles to changes in flow velocity and the ability of particles to follow turbulent fluctuations have been considered by Melling (1985). Bryanston-Cross and Epstein (1990) have looked at the particular case of transonic flows and the ability of particles to respond to step changes in velocity, such as those found in shock waves.

For a particle to follow the change in velocity induced by a normal shock, with upstream Mach number 1.2, a particle of specific gravity 1 and on the order of 0.5-μm diameter is required. To follow 10 kHz turbulence to within 1%, Melling (1985) determined that a particle size of 0.8 μm and specific density 1 is required. Polystyrene latex particles, held in suspension before use in an alcohol solution, have found considerable application in terms of seeding material. Seegmiller (1985) considered the challenges associated with introducing seeding into subsonic, transonic, and supersonic flows in some detail, checking, in particular, the requirements to ensure that the carrier solution had evaporated by the time that the measurement zone had been reached. The proceedings of a workshop held at the NASA-Langley Research Center in 1985 (Hunter and Nicols 1985) is a particularly useful source covering a wide range of problems.

The implications of particle dynamics cannot be considered in isolation. Not only must the particles follow the flow, they must also scatter sufficient light to enable detection. However, DGV is not reliant upon imaging individual scattering sites, because in reality, each CCD pixel images a number of particles dependent on the seeding density and magnification of the imaging system. Nevertheless, particle scattering efficiency is critical in establishing the required laser power and seeding concentration. For particles on the order of 1 μm in diameter, light scattering is dictated by the Mie theory (see for example, van de Hulst 1957). Extensive calculations based on this theory were conducted by Ainsworth and Thorpe (1994) in order to assess the impact of particle size, refractive index, and scattering angle. Perhaps of greatest interest to DGV measurements is the effect of scattering angle, because this is a relatively free parameter when laying out the experiment. Scattering is strongest in the forward direction and reasonably strong in the side- and back-scatter directions. These forward and back-scatter extremes are of little use to DGV measurements, because viewing must occur at an oblique angle to the light sheet in order to provide global measurements. In the case of 0.5-μm diameter particles, two minima occur in the side-scatter angles and could have a deleterious consequence on the required illumination intensity and/or recording medium sensitivity.

Bryanston-Cross and Epstein (1990) found, in their PIV work, that a satisfactory image of one polystyrene seeding particle of 0.5-μm diameter could be obtained with a 10–20 mJ pulse of energy (supplied in his case by a Nd:YAG laser) using TMAX 3200 film. This bodes well for DGV where the light from a number of particles is imaged onto a single pixel. A seeding density of 10–15 particles per cubic mm was optimum in PIV at velocities up to 450 ms^{-1} velocity, yielding 1000 particle image pairs for each photographic (35-mm) frame. Other useful references include Melling (1985), who makes recommendations on particle generators and sizing methods, and Strazisar (1985), who contemplates the use of a liquid fluorescing seed to increase light output, formed by dissolving an organic dye in benzyl alcohol and ethylene alcohol (tailored to the argon ion green line).

Because DGV measurements are at a much earlier stage of development than those obtained using PIV, most of the measurements detailed in the next section have been made with less exotic seeding materials. Komine's original work (1991) used 1.5-μm diameter seeding generated by a Laskin generator, using olive oil as the seeding material, pressurised by dry nitrogen. The oil aerosols were injected into a small table-top wind tunnel at one end through a small nozzle. Meyers (1992), examining the flow over a 75° delta wing in his wind tunnel, used propylene glycol vapourisation as a means of seeding. The particles, with a size distribution peaking at 0.7 μm with a tail to 10 μm, were injected upstream of a honeycomb calming region. Komine et al. (1994) present calculations of seeding requirements for DGV in a flight-based system, using existing smoke bomb generators, and concludes that the reflected energy will not be a problem for detection for laser energies of the order of 0.1 J/pulse. Bryanston-Cross and Epstein (1990) work would seem to confirm this. Roehle and Schodl (1994) used glycerol/ethanol particles generated using a Laskin nozzle, with a particle size of less than 1 μm, bigger particles being suppressed by an impactor. Thorpe et al. (1995) again used a Laskin-type generator, this time seeded with glycerine and water. No other information is available from the other published DGV measurements given below.

It seems, therefore, that the requirements for laser power and seeding concentration required for successful imaging of the flow field are less stringent for DGV than for PIV. For transonic flows, particle diameters of 0.5 μm or less are required. Flexibility in matching the camera dynamic range to the variation in light intensity across the illuminated area is possible by use of apertures incorporated in the imaging system, by altering the integration period, and by adjusting the laser power.

Published Doppler global velocimetry system results

Whilst DGV systems have been used to measure gross aerodynamic features around aircraft intakes and aerofoil configurations by workers based at NASA, this section is confined to measurements in simpler velocity fields that have well-known results. By this means, verification of the effectiveness and integrity of the alternative DGV techniques in use can be assessed.

Rotating discs

Rotating discs illuminated by an argon ion laser have been used by a number of workers to provide known Doppler shifts, and attempts using this test vehicle are described below.

Chan et al. (1995b) published their work on a spinning disc and initially experienced some difficulties in aligning their im-

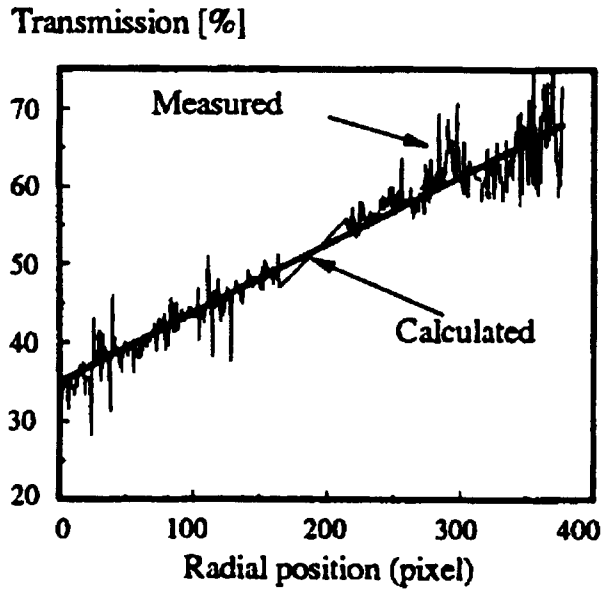

Figure 18 Rotating-disc measurement: variation of intensity ratio (hence velocity) with pixel position (Chan et al. 1995b)

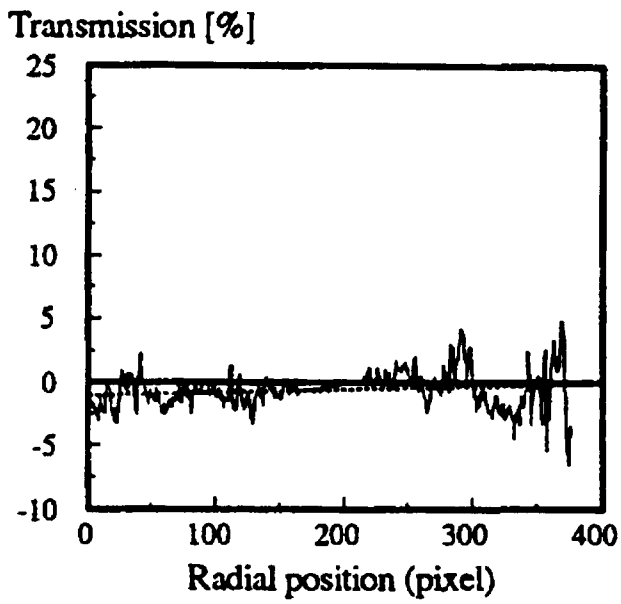

Figure 19 Smoothing of high-frequency noise in Figure 18, using spatial averaging (Chan et al. 1995b)

ages. A high surface speed was achieved using an air motor (maximum speed 80,000 rpm) attached to an acrylic disc 75-mm diameter, 3-mm thick. Rim speeds of 120 ms^{-1} were achieved. High-frequency noise content in the processed image was evident, and ultimately, they used two filtering techniques, a spatial averaging filter, and a median filter, to reduce this. The noise was thought to be due to misalignment of the two images during signal normalisation and by the surface roughness of the disc. A line plot of image intensity ratio (transmission) *versus* radial position is given in Figure 18 showing the expected linear variation of velocity with radius. The deviation of the transmission from this linear variation after processing with the spatial averaging technique to reduce high-frequency noise is shown in Figure 19.

The equivalent measurement made at Cranfield by Ford and Tatam (1994) is shown in Figure 20. Here, a wheel of 100-mm diameter was used, spinning at 105 Hz. Tip velocity was of order 29 ms^{-1}. It should be noted that the data presented in this figure are the average of 45 dataframes, so unwanted noise will have been reduced.

Meyers (1994) demonstrates the use of a three-velocity component system (using three DGV receiver optical systems; six

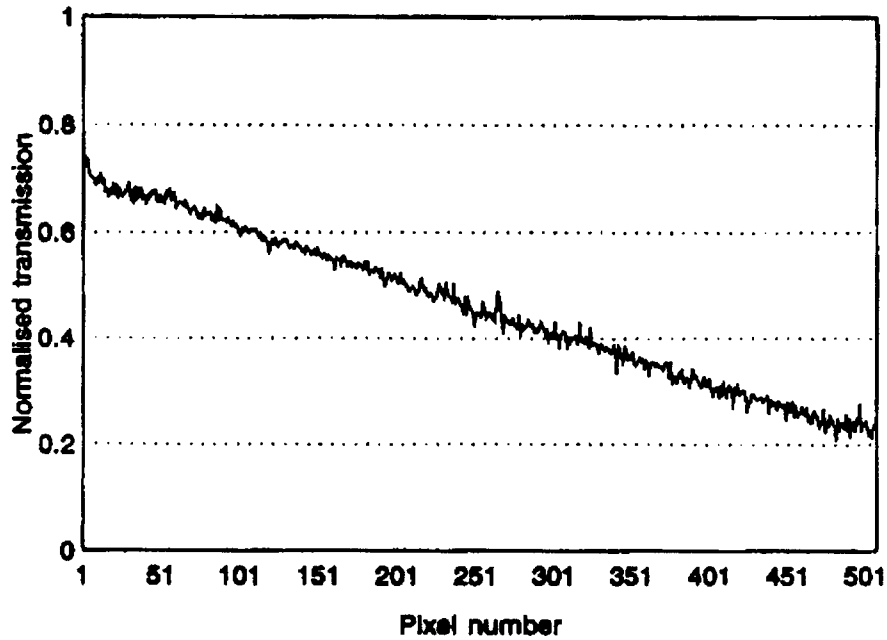

Figure 20 Rotating-disc data of Ford and Tatam; average of 45 shots (Ford and Tatum 1994)

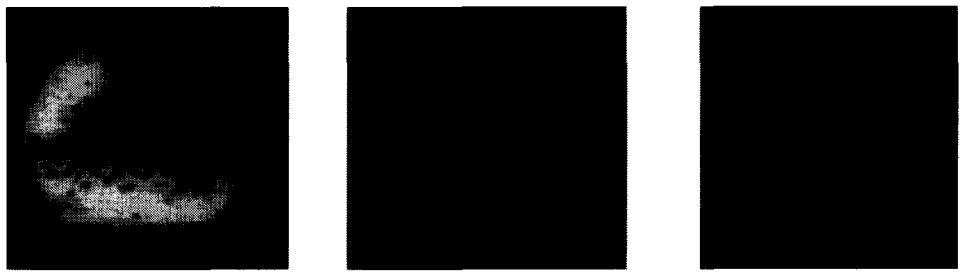

Figure 21 Three components of velocity (rotating disc) derived by Meyers (1995) from three separate DGV optical receivers

cameras in their technique) mounted to survey the velocity field of a spinning disc. The three receiver optical systems were placed to the left, right, and above the disc, all at 30° angle to the plane of the disc. The wheel was illuminated with a cone of laser light propagating in the horizontal plane, inclined at 45° to the disc. The data images of the three conventional u,v,w components are shown in Figure 21, no lone data are available. "As expected, the u component was nominally 0 ms^{-1}, and the v and w components had the appropriate profiles for a solid body of revolution," Meyers (1995).

In the Oxford work, a disc of radius 65-mm was used, typically producing a tip speed of 40 ms^{-1}. The geometrical layout of the laser, disk, and imaging system (Thorpe et at. 1995) is shown in Figure 22—the measured velocity component is also shown and lies at an angle of 40° to the disk rotational axis. This geometry is such that the DGV is sensitised to the horizontal velocity of the disk. The laser beam is expanded using a single spherical lens and projected onto the disk. The signal and reference portions of the acquired image are separated and divided to provide the ratio map shown in Figure 23. Because the Oxford system uses the second (laser monitoring) iodine cell, it is possible to produce velocity directly from the measured data. A plot of the velocity vertically down one pixel row which passes through the centre of the disk is given in Figure 24. Note: these data are the result of one acquired image and do not use digital filtering to smooth the high-frequency structure. The velocity varies linearly across the disc, within a tolerance of ± 2 ms^{-1}. The areas of high noise in this plot should be ignored, because they relate to signals from outside the disc area. The high-frequency noise on the signal relates to shadowing of geometrical features on the face of the disc, which would require a higher pixel resolution to remove. There is a hole at the centre of the disc, which, of course, cannot scatter light, and therefore, produces an erroneous signal in the whole field.

Finally, because so much is made in the literature of the use of a rotating disc to verify system alignment, a note of caution is introduced. In fact, it is a very benign test case. Velocity (and, hence, intensity) gradients are gradual, rather than abrupt, hence, misalignment will not be critical. This is demonstrated by processing the results from a synthesised rotating disc velocity field. A Gaussian illumination profile was assumed, and pseudosignal and reference images were deliberately misaligned by controlled amounts. The error in velocity is seen to be small, even with a 0.1 pixel misalignment in the vertical sense, Figure 25. The same would not be true for a flow field with steep velocity (and, hence, intensity) gradients, as will be demonstrated below for an open jet.

Subsonic open-jet flow field

A second test case which has a velocity field well established in the literature is that of the subsonic open jet. Meyers (1995) again used a three-component DGV system this time to show measurements made at NASA-Ames of the streamwise velocity component 0.25 jet diameters downstream of a 220-mm diameter jet, Figure 26. The jet operated at temperatures up to 700°C and velocities over 500 ms^{-1}.

Komine et al. (1994) have also used an open-jet configuration. In their case, a laminar-flow subsonic jet was used, with a 3×3-inch section nozzle. Exist velocities of 70, 100, 125, and 150 ms^{-1} were used, and measurements made with pitot probes, a commercial LDA system, and the DGV system with Nd:YAG illumination. Unfortunately, the LDA data showed considerable discrepancy with the pressure-probe data, thought to be due to seeding difficulties and the production of large particles. In the end, the DGV results were compared with the pitot-probe results, although ultimately there was still a large discrepancy between pitot-probe and DGV measurement.

Roehle and Schodl (1994) tested the principles of the DGV technique on an open jet, but not using the whole-field capability —they did not use an imaging system. Rather, they used point detectors (photodiodes). They again used the velocity field at the exit of a free jet, seeded as described above. They compared their measurements with results from L2F. The flow speed was varied between 40 and 130 ms^{-1}. In general, the results are good (Figure 27), with a mean difference between the two techniques of ± 3 ms^{-1}.

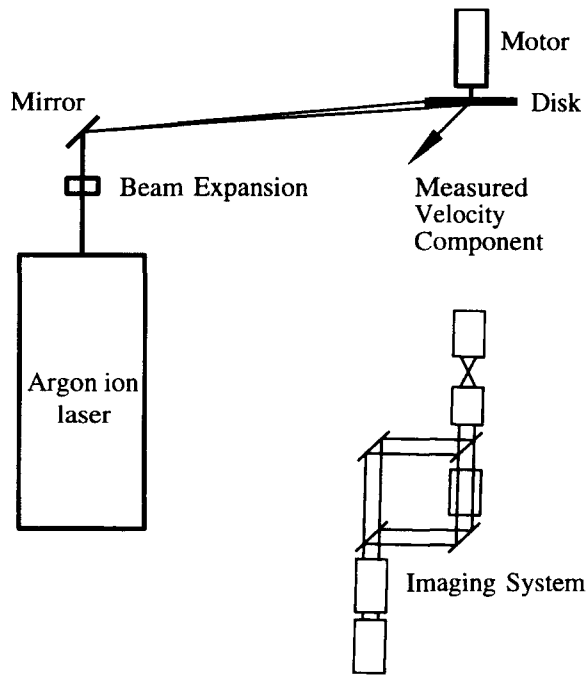

Figure 22 Optical DGV system used by Thorpe et al. (1995) for rotating disc work

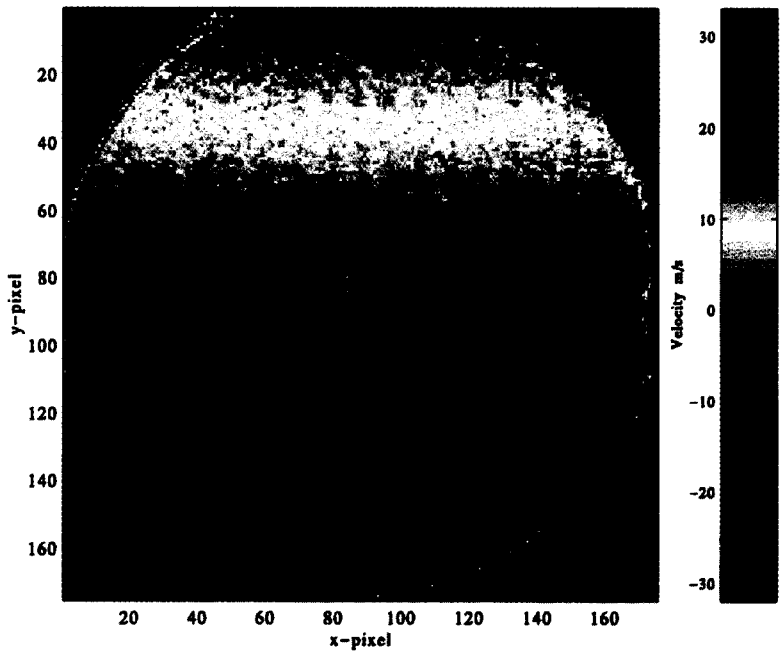

Figure 23 Pseudocolour representation of velocity field measured on rotating disc, simultaneously measuring laser frequency (Thorpe et al. 1995)

Finally, Thorpe et al. (1995) also used an open-jet experiment —this time a contoured convergent nozzle, 12-mm in exit diameter. The jet was seeded as described above. Two measurement geometries were used, shown in Figures 28 and 29. In the first, the laser light sheet (1×50 mm) propagated directly along the jet longitudinal axis. The optical recording system was placed normal to this light sheet, at a working distance of 0.7 m. Each pixel was equivalent to an area of 0.25×0.25 mm of flow field. The measured component of velocity was, thus, at 45° to the jet axis.

In the second configuration, the illuminating sheet and optical receiving system remained invariant, and the jet axis was moved to lie at 45° to the light sheet. Thus, the system now measured jet axial velocity directly, illuminating a transverse cross section of the jet. One pixel was now equivalent to an area of 0.37 mm $\times$ 0.37 mm of flow field.

Results were obtained at a jet exit velocity of 62 ms^{-1}, at a variety of axial locations, and seem to be a most convincing demonstration of the technique. A small fraction of the data are shown in Figure 30, both as gray-level representations and line plots. The line plots are compared with the correlations of Gauntner et al. (1970)—a compendium of considerable data from a variety of sources—and the rms deviation is as low as 2.5 ms^{-1}. The conclusion of this work was that "DGV has proved capable of acquiring data of high quality from individual data images... excellent agreement with a correlation from the literature. The error estimates for the DGV measurements, based on fundamental measurement uncertainties, were found to be generally in agreement with the deviation of the measurements from the correlation." Thorpe et al. 1995.

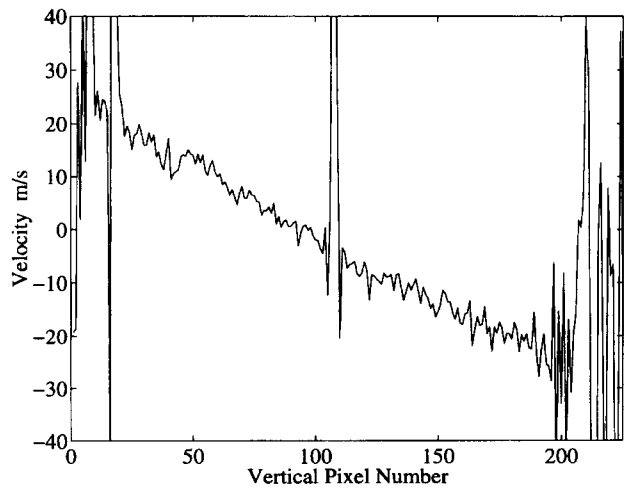

Figure 24 Line plot of velocity as determined by one vertical pixel row, from the data in Figure 23 (Thorpe et al. 1995)

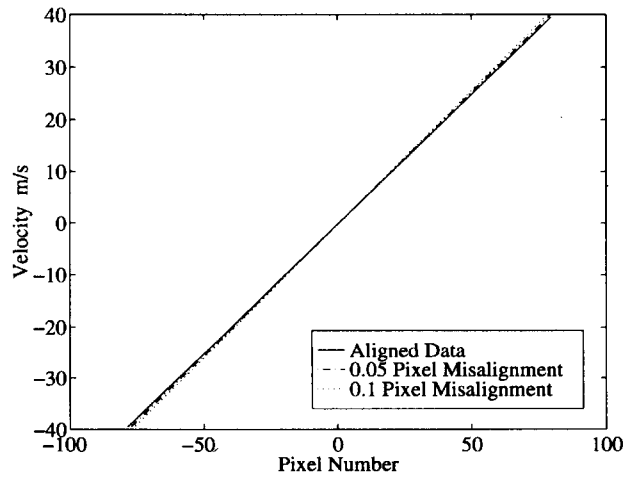

Figure 25 Small error in velocity field caused by image misalignment, illustrating the benign nature of a rotating-disc test field

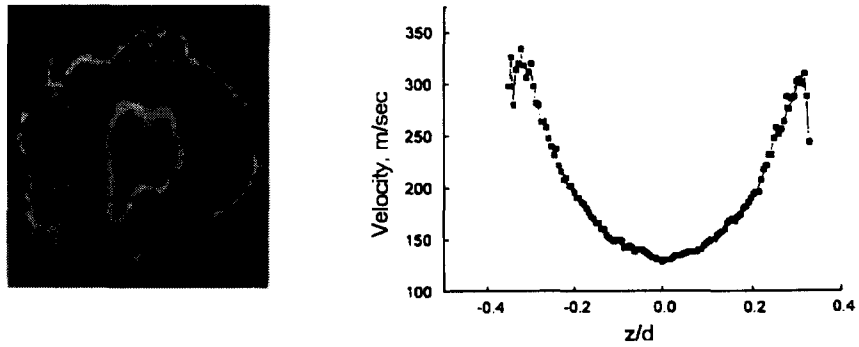

Figure 26 Jet measurement of Meyers (1995)

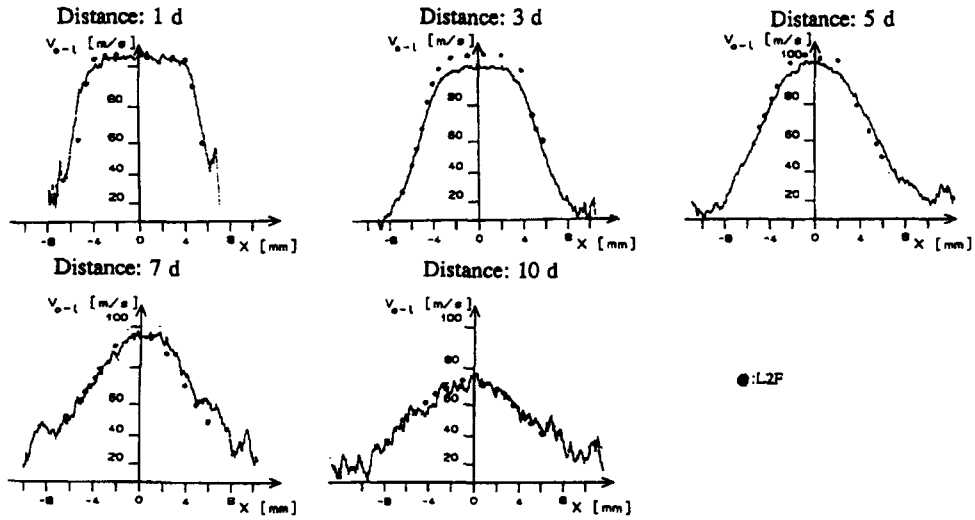

Figure 27 Jet measurement of Roehle and Schodl (1994), using the measured Doppler shift, but analysed by photodiode rather than whole field; compared with L2F measurements

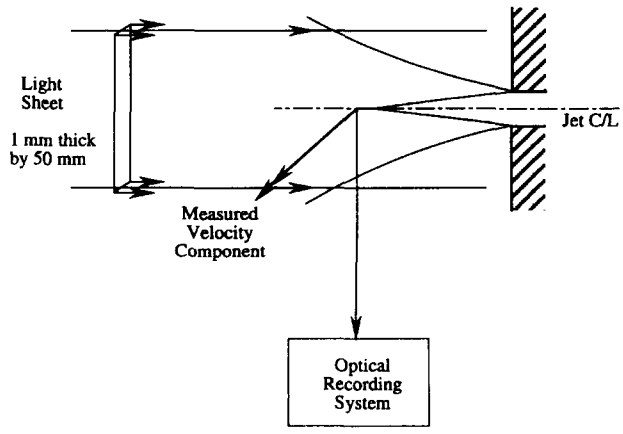

Figure 28 Measurement system used for jet axis measurement (Thorpe et al. 1996)

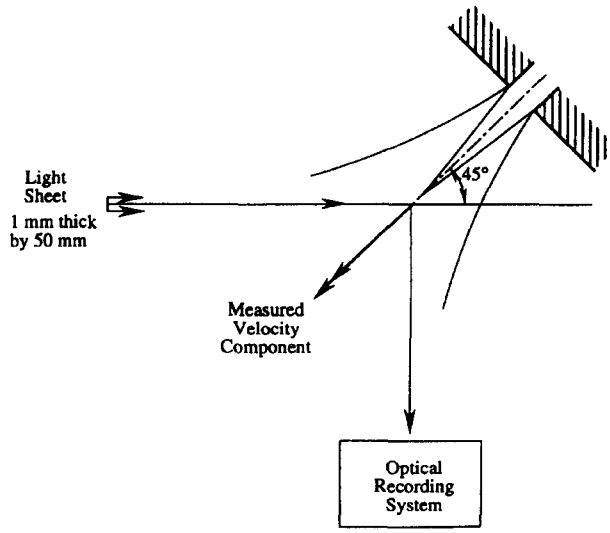

Figure 29 Measurement system used for jet cross section measurement (Thorpe et al. 1996)

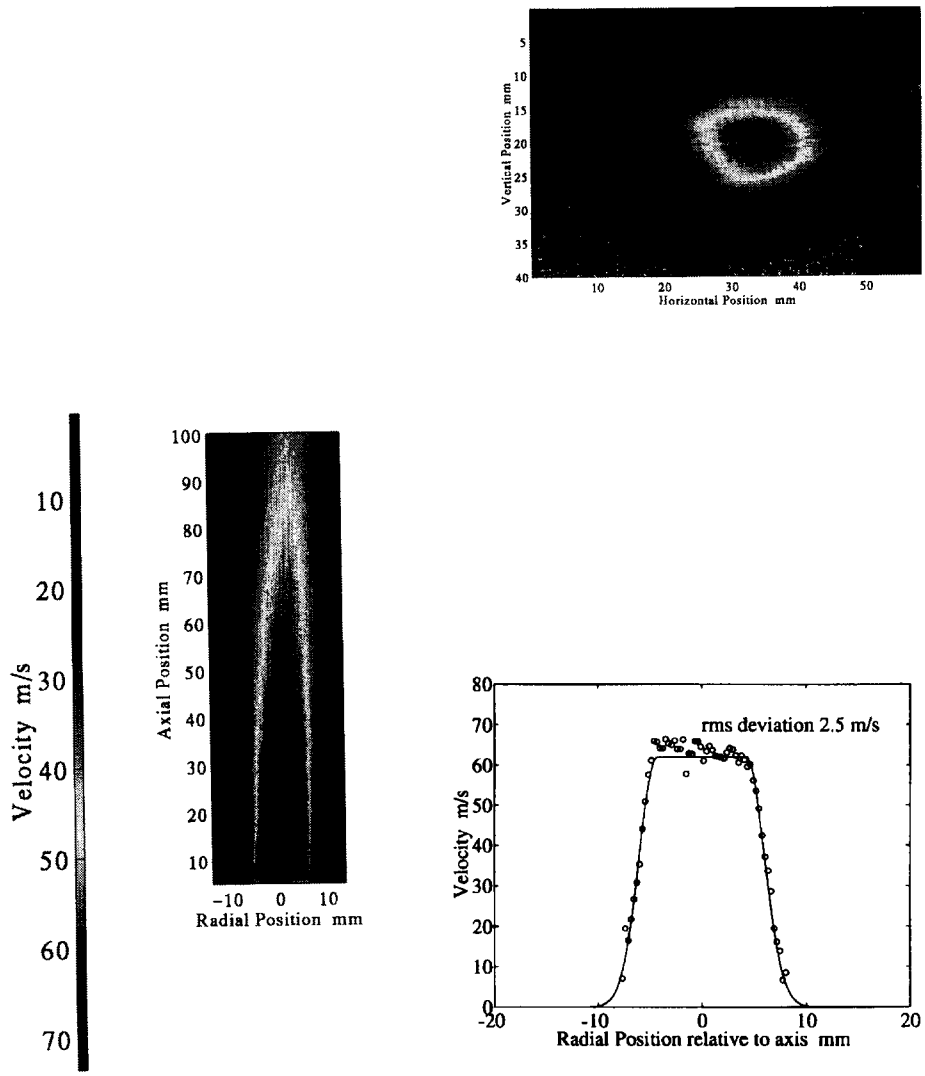

Figure 30 Doppler global velocimetry measurement in an open-jet flow field; axial and cross-sectional distribution of jet axial velocity and comparison with literature correlations (Thorpe et al. 1996)

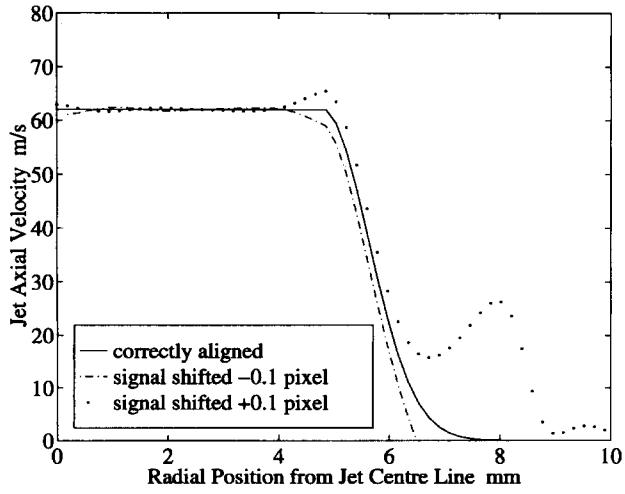

Figure 31 Synthetic jet; signal and reference images displace by 0.1 pixel

Finally, in the manner described above for the rotating disc, the images from a synthesised open jet were created, using the literature correlation for the velocity and a measured intensity profile for the base reference image. Again, the pseudosignal and reference images were deliberately misaligned, by 0.1 pixels (Figure 31). Now, the errors in the mixing region of the jet become significant with pixel misalignment, demonstrating that the open-jet flow field represents a challenging test for the DGV technique.

Conclusions

The technique of DGV, pioneered in its original form by Komine, and the differing technology employed by a number of investigators in its application have been described and compared. Comparisons have been made with the other major whole-field technique, PIV, a technique of considerably older lineage. Examples of DGV measurements made in standard test cases have been reviewed in their own right and in comparison with literature

correlations. It remains the authors' view that considerable excitement should continue to greet work in this field, with accurate 3-D whole-field measurements becoming a matter of routine in due course.

Acknowledgment

The support from the EPSRC in the form of grant GR/J54307 is gratefully acknowledged.

References

Adrian, R. J. 1991. Particle-imaging techniques for experimental fluid mechanics. *Ann. Rev. Fluid Mech.*, **23**, 261–304

Ainsworth, R. W. and Thorpe, S. J. 1994. The development of a Doppler global velocimeter for transonic turbine applications. *Proc. ASME Int. Gas Turbine and Aeroengine Congress and Exposition*, (ASME paper 94-GT-146), The Hague

Bryanston-Cross, P. J. and Epstein, A. 1990. The application of sub-micron particle visualisation for PIV(particle image velocimetry) at transonic speeds, *Prog. Aerospace Sci.*, **27**, 237–265

Chan, V. S. S., Heyes, A. L., Robinson, D. I. and Turner, J. T. 1995a. Iodine absorption filters for Doppler global velocimetry. *Meas. Sci. Technol.*, **6**, 784–794

Chan, V. S. S., Robinson, D. I., Turner, J. T. and Heyes, A. L. 1995b. A simplified Doppler global velocimeter. *Proc. ASME/EALA 6th Int. Conference on Laser Anemometry Advances and Applications*, Hilton Head, SC

Ford, H. D. and Tatam, R. P. 1994. Real-time Doppler global velocimetry. *Proc. Meeting on Engineering Applications of Optical Diagnostic Techniques*, Cranfield University, UK

Gauntner, G. W. Livingood, J. N. B. and Hrycak, P. 1970. Survey of literature on flow characteristics of a single jet impinging on a flat plate. NASA TN D-5652

Gill, P. 1979. Iodine saturation spectroscopy for multi-wavelength stabilisation of an argon/krypton ion laser. *Metrologia*, **15**, 117–123

Hunter, W. W. and Nichols, C. 1985. *Wind-Tunnel Seeding for Laser Velocimeters, Proc. Workshop at NASA Langley*, NASA Conference Publication 2393

Komine, H. and Brosnan, S. J. 1991. Instantaneous, three-component, Doppler global velocimetry. *Proc. ASME 4th Int. Conference on Laser Anemometry, Advances and Applications*

Komine, H., Brosnan, H., Litton, A. B. and Stappaerts, E. A. 1991. Real-time, Doppler global velocimetry. *Proc. AIAA 29th Aerospace Sciences Meeting*, AIAA paper, 91-0337) Reno, NV

Komine, H., Brosnan, H., Long, W. H. and Stappaerts, E. A. 1994. Development of a flight research instrumentation system for application to noninstrusive measurements of the flow-field. NASA CR 191490

Lee, S. J., Chung, M. K., Mun, C. W. and Cho, Z. H. 1987. Experimental study of thermally stratified unsteady flow by NMR-CT. *Exp. Fluids.*, **5**, 240–246

Manners, R. J., Thorpe, S. J. and Ainsworth, R. W. 1996. Image processing techniques for Doppler global velocimetry. *Proc. I. Mech. E. Conference on Optical Methods and Data Processing in Heat and Fluid Flow*, London

McKenzie, R. L. 1996. Measurement capabilities of planar Doppler velocimetry using pulsed lasers. *Appl. Optics*, **35**, 948–964

Melling, A. 1985. Seeding gas flows for laser anomometry. AGARD CP 399, paper 15

Meyers, J. F. 1992. Doppler global velocimetry—The next generation? *Proc. AIAA 17th Aerospace Ground Testing Conference*, (Paper 92-3897), Nashville, TN

Meyers, J. F. 1994. Development of Doppler global velocimetry for wind-tunnel testing. *Proc. AIAA 18th Aerospace Ground Testing Conference*, (Paper 94-2582), Colorado Springs, CO

Meyers, J. F. 1995. Development of Doppler global velocimetry as a flow diagnostic tool. *Meas. Sci. Technol.*, **6**, 769–783

Meyers, J. F. and Komine, H. 1991. Doppler global velocimetry: A new way to look at velocity. *Proc. 4th Int. Conference on Laser Anemometry, Advances and Applications*

Meyers, J. F., Lee, J. W. and Cavone, A. A. 1991. Signal processing schemes for Doppler global velocimetry. *Proc. IEEE 14th Int. Congress on Instrumentation in Aerospace Simulation Facilities*, Rockville, MD, 321–328

Miles, R. B., Connors, J. J., Markovitz, E. C., Howard, P. J. and Roth, G. J. 1989. Instantaneous profiles and turbulence statistics of supersonic free shear layers by Raman excitation plus laser-induced electronic fluorescence (relief) velocity tagging of oxygen. *Exp. Fluids*, **8**, 17–24

Roehle, I. and Schodl, R. 1994. Evaluation of the accuracy of the Doppler global technique. *Proc. I. Mech. E. Conference on Optical Methods and Data Processing in Heat and Fluid Flow*, London

Seegmiller, H. L. 1985. Seeding subsonic, transonic, and supersonic flows with 0.5-micron polystyrene spheres. In *Wind-Tunnel Seeding for Laser Velocimeters, Proc. Workshop at NASA-Langley*, NASA CP 2393.

Strazisar, A. J. 1985. Laser fringe anemometry. AGARD CP 399, paper no. 6

Thorpe, S. J., Ainsworth, R. W. and Manners, R. J. 1995. The development of a Doppler global velocimeter and its application to a free jet flow. *Proc. ASME/EALA 6th Int. Conference on Laser Anemometry Advances and Applications*, Hilton Head, SC, USA

Thorpe, S. J., Ainsworth, R. W., and Manners, R. J. 1996. Time-averaged free-jet measurements using Doppler global velocimetry. *Proc. ASME Symposium on Laser Anemometry and Experimental and Numerical Flow Visualisation*, San Diego, CA, USA

Usry, J. W., Meyers, J. F. and Miller, L. S. 1992. Doppler global velocimeter measurements of the vortical flow above a thin delta wing. AIAA paper 92-0005

van de Hulst, H. C. 1957. *Light Scattering by Small Particles*, Wiley, New York

Wolberg, G. 1992. *Digital Image Warping*, IEEE Computer Society Press, New York

Yeh, Y. and Cummins, H. Z. 1964. Localised fluid-flow measurements with a He–Ne laser spectrometer. *Appl. Phys. Lett.* **4**, 176–178